JACS
JOURNAL OF THE AMERICAN CHEMICAL SOCIETY

Communication

pubs.acs.org/JACS

$CoSe_2$ Nanoparticles Grown on Carbon Fiber Paper: An Efficient and Stable Electrocatalyst for Hydrogen Evolution Reaction

Desheng Kong,[†] Haotian Wang,[‡] Zhiyi Lu,[†,#] and Yi Cui*[,†,§]

[†]Department of Materials Science and Engineering, and [‡]Department of Applied Physics, Stanford University, Stanford, California 94305, United States

[#]State Key Laboratory of Chemical Resource Engineering, Beijing University of Chemical Technology, Beijing 100029, China

[§]Stanford Institute for Materials and Energy Sciences, SLAC National Accelerator Laboratory, 2575 Sand Hill Road, Menlo Park, California 94025, United States

Supporting Information

ABSTRACT: Development of a non-noble-metal hydrogen-producing catalyst is essential to the development of solar water-splitting devices. Improving both the activity and the stability of the catalyst remains a key challenge. In this Communication, we describe a two-step reaction for preparing three-dimensional electrodes composed of $CoSe_2$ nanoparticles grown on carbon fiber paper. The electrode exhibits excellent catalytic activity for a hydrogen evolution reaction in an acidic electrolyte (100 mA/cm^2 at an overpotential of ~180 mV). Stability tests though long-term potential cycles and extended electrolysis confirm the exceptional durability of the catalyst. This development offers an attractive catalyst material for large-scale water-splitting technology.

Hydrogen generation through electrolysis of water offers an attractive avenue to store energy from renewable sources such as the sun.[1,2] Many solar water-splitting devices are designed to function in acidic electrolyte, in which the state-of-the-art hydrogen-producing catalysts are based on noble metals like Pt. The scarcity of Pt makes it impractical for global-scale applications.[1−3] It is therefore attractive to develop low-cost, acid-stable alternatives that are suitable for water splitting; a few successful examples are MoS_2,[4−12] $MoSe_2$,[13,14] WS_2,[15] WSe_2,[14] MoB,[16] Mo_2C,[17] $NiMoN_x$,[18] Ni_2P,[19] and $Co_{0.6}Mo_{1.4}N_2$.[20] We recently introduced first-row transition-metal dichalcogenides as a new group of high-performance hydrogen evolution reaction (HER) catalysts, by measuring metal dichalcogenide thin films prepared through selenization/sulfurization of e-beam-evaporated metal films.[21] These catalysts exhibit high activity toward HER. The practical application of these catalysts, however, is still hindered by the costly and low-throughput preparation procedures, involving metal film deposition under high vacuum. In this study, we develop a facile synthesis approach to grow $CoSe_2$ nanoparticles on high-surface-area electrodes. The catalyst displays high activity for HER and excellent stability, which is readily integrated into photoelectrochemical hydrogen production devices.

First-row transition-metal dichalcogenides have been extensively studied as a family of active catalysts for oxygen reduction reaction (ORR) in acidic electrolyte.[22−24] Recently, their high activity for HER has been directly identified in experiments.[21,25,26] Within these catalysts, $CoSe_2$ displayed the optimal activity, demonstrating it to be among the most active electrocatalysts based on non-noble metals. As shown in Figure 1a, these metal dichalcogenides exist in cubic pyrite-type or orthorhombic macarsite-type structures, where the metal atoms are octahedrally bonded to adjacent chalcogen atoms. The subtle structural distinction is mainly associated with the octahedral linkage. The octahedra are corner-shared in pyrite and edge-shared in macarsite.[27] In our previous study, these transition-metal dichalcogenides were prepared by converting

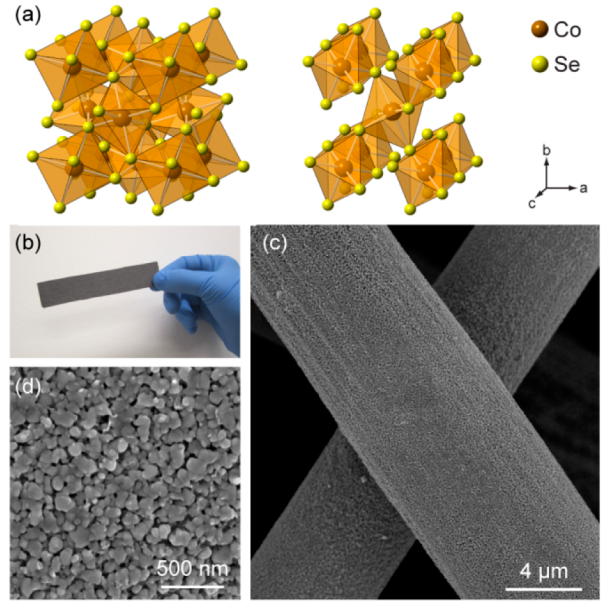

Figure 1. (a) Crystal structure of $CoSe_2$ in cubic pyrite-type phase (left) and orthorhombic macarsite-type phase (right), in which Co and Se are displayed in orange and yellow, respectively. (b) Photograph of as-prepared $CoSe_2$ catalyst on a piece of 1.5 cm × 10 cm carbon fiber paper. (c) SEM image of a layer of $CoSe_2$ catalyst grown on carbon fiber paper. (d) High-resolution SEM image revealing the structure of $CoSe_2$ coating, consisting of nanoparticles in dimension of tens of nanometers.

Received: February 12, 2014
Published: March 14, 2014

   dx.doi.org/10.1021/ja501497n | J. Am. Chem. Soc. 2014, 136, 4897−4900

from e-beam-evaporated metal thin films through a sulfurization/selenization reaction.[21] Although the process allows easy access to high-quality dichalcogenide films, it is likely too costly to be deployed for large-scale applications.

In this study, we introduce a new approach to grow $CoSe_2$ catalysts by preparing cobalt oxide nanoparticles on carbon microfiber paper, followed by selenization under Se vapor (details available in Supporting Information). These cobalt oxide nanoparticles are obtained by pyrolysis of a precursor ink consisting of cobalt nitrate and polyvinylpyrrolidone dissolved in dimethylformamide, which is applied onto the electrode through a drop-casting process. This synthesis procedure is compatible with sizable electrodes, limited only by the dimension of the tube furnace reactor. For example, Figure 1b presents a digital photo of 1.5 cm ×10 cm carbon fiber paper (CP) loaded with $CoSe_2$ catalyst by reactions in a 1-in.-diameter tube furnace reactor. In addition, the process also allows facile preparation of HER catalyst on various electrodes. We employed scanning electron microcopy (SEM) to study the microstructure of as-grown $CoSe_2$ catalysts on CP and silicon wafer, respectively. Figure 1c illustrates the catalyst prepared on commercial CP (2050A, from Fuel Cell Store Inc.), in which the carbon fibers are conformally covered with a layer of nanoparticulate $CoSe_2$ film. CP is a porous three-dimensional (3D) electrode consisting of carbon fiber of ∼8 μm in diameter (see Figure S2). The highly textured surface of the carbon fiber facilitates the nucleation and growth of a catalyst layer with strong mechanical interaction. Apparently, the synthesis procedure allows facile preparation of a catalyst coating layer on 3D electrode with complicated geometry, which is frequently employed in solar water-splitting devices.[1,28−33] High-magnification SEM images (Figure 1d) further reveal that the catalyst layer consists of densely packed $CoSe_2$ nanoparticles in the dimension of tens of nanometers. The overall structure of the $CoSe_2$ catalyst layer on silicon wafer is quite similar, being also formed by packed $CoSe_2$ nanoparticles (see Figure S3). The $CoSe_2$ layer on these electrodes serves as a binder-free catalyst coating that can be readily used for electrochemical studies. Notice that the synthesis approach is generally applicable to other metal chalcogenides, exemplified by the formation of $NiSe_2$ nanoparticles over CP with similar procedures (see Figures S6 and S7).

Additional structural characterizations are acquired by X-ray diffraction (XRD) and Raman spectroscopy. In Figure 2a, XRD spectra were recorded at each synthesis step. In the first reaction step, pyrolysis of precursor ink at 600 °C yields oxide in a rocksalt-structure cobalt monoxide (CoO) phase (ICDD PDF no. 00-048-1719). The following selenization step converts most of the oxide into $CoSe_2$ in cubic pyrite-structure phase (ICDD PDF no. 04-003-1990), whereas a small fraction of $CoSe_2$ in macarsite-structure phase (ICDD PDF no. 00-053-0449) is also observed. The structural similarity and the small lattice mismatch between the two phases allow epitaxial growth of macarsite on pyrite,[34] which is widely observed in experiments.[23,35] In addition, Raman spectra of as-grown catalyst on CP and silicon wafer are shown in Figure 2b with consistent spectral features, suggesting the film quality is less sensitive to the choice of the substrates. The sharp peak at 190 cm^{-1} corresponds to the Se−Se stretching mode of cubic $CoSe_2$,[22,36] whereas the broad peak around 250 cm^{-1} is associated with amorphous Se.[37] Previous studies suggest the Raman-active mode of orthorhombic phase is difficult to observe in experiment, which is consistent with our result.[38]

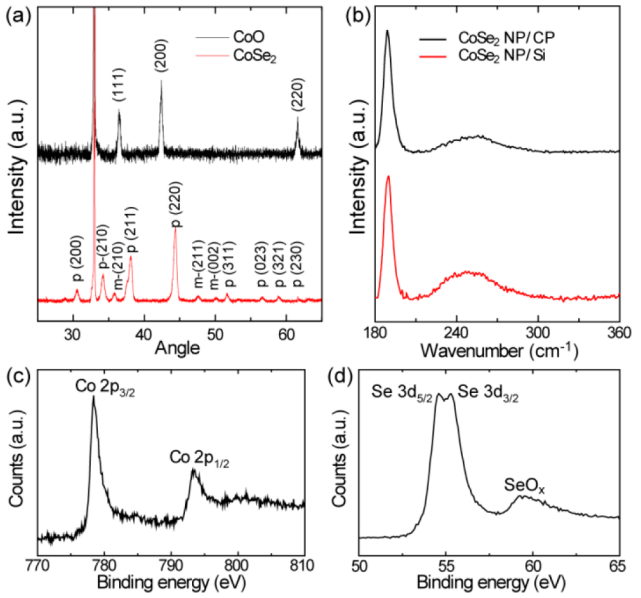

Figure 2. (a) XRD spectra from the sample at each synthesis step, revealing the formation of CoO through pyrolysis followed by $CoSe_2$ through selenization. (b) Raman spectra from $CoSe_2$ nanoparticles grown on carbon fiber paper and silicon wafer. High-resolution XPS spectra of (c) Co 2p and (d) Se 3d region.

The activity of HER catalyst is expected to be sensitive to the valence state and coordination environment of the metal center.[11,20] For first-row metal dichalcogenides, the low-spin, divalent metal cations are octahedrally coordinated with S_2^{2-} or Se_2^{2-} dimers.[39−41] In Figure 2c, our X-ray photoelectron spectroscopy (XPS) data reveal the electron-binding energies of Co $2p_{3/2}$ at 778.4 eV and Co $2p_{1/2}$ at 793.3 eV, which correspond to Co^{2+} cations in $CoSe_2$.[38,42] In Figure 2d, the binding energies of Se $3d_{5/2}$ and $3d_{3/2}$ at 54.6 and 55.3 eV, respectively, are also consistent with $CoSe_2$.[38] We notice that the d-electron configuration of metal cations largely impacts the physical properties of these metal dichalcogenides. The 3d bands arising from the metal atoms further split into t_{2g} and e_g sub-bands by a crystalline field. For $CoSe_2$, the Co 3d electrons adopt a low-spin configuration in the form of $t_{2g}^6e_g^1$, which makes $CoSe_2$ a metallic conductor.[43] The metallic property of $CoSe_2$ permits efficient transport of charge from the electrode to the surface of the catalysts, which is desired for high-performance electrocatalysts.

The activity of our catalyst is evaluated in a typical three-electrode cell setup with 0.5 M H_2SO_4 electrolyte. The $CoSe_2$ nanoparticles grown on CP and glassy carbon (GC) electrodes are employed as the working electrodes. As shown in Figure 3a, nanoparticles grown on CP exhibit much higher activity than those on GC, benefiting from the 3D structure of CP. The overpotentials required to drive cathodic current densities of 10, 20, and 100 mA/cm^2 are 137, 150, and 181 mV, respectively. These overpotentials are among the most active for electrocatalysts based on non-noble materials (see Table S2). Among the $CoSe_2$ nanoparticle/CP electrodes tested in our study, their HER activities are also highly consistent (see Figure S4 and Table S1). In contrast, CP exhibits negligible HER activity in the measurement voltage range, which further confirms that the high activity of the catalyst paper comes from the coating layer of $CoSe_2$ nanoparticles. In Figure 3b, the corresponding Tafel plots (log j_g vs E) reveal small Tafel slopes

dx.doi.org/10.1021/ja501497n | J. Am. Chem. Soc. 2014, 136, 4897−4900

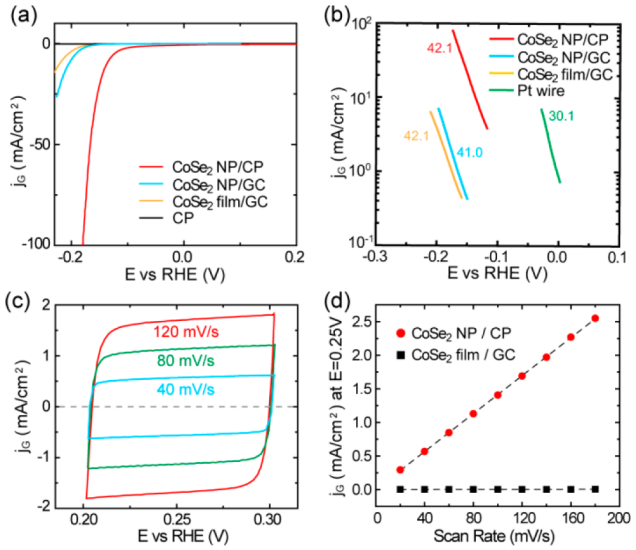

Figure 3. (a) Polarization curves of $CoSe_2$ nanoparticle (NP)/carbon fiber paper (CP) electrode in 0.5 M H_2SO_4, along with $CoSe_2$ NP/glassy carbon (GC), $CoSe_2$ film/GC, and CP for comparison. (b) Corresponding Tafel plots in comparison with a Pt wire. (c) Cyclic voltammograms (CV) are taken in a potential window without faradaic processes. (d) The capacitive currents at 0.25 V vs RHE as a function of scan rate for $CoSe_2$ NP/CP and $CoSe_2$ film/GC electrodes.

of ~40 mV/dec for $CoSe_2$ nanoparticle-based electrodes. This suggests that the HER occurs through a Volmer–Heyrovsky mechanism, in which a fast discharge of a proton is followed by rate-limiting electrochemical recombination with an additional proton.[44,45] The Tafel slopes of the $CoSe_2$ nanoparticle-based electrodes are consistent with the value for a $CoSe_2$ film. This suggests a similar surface chemistry in HER, as these catalysts are formed by similar selenization reactions. Non-precious HER catalysts usually exhibit Tafel slopes ranging from 40 to 120 mV/dec.[6,7,9,13,14,19] The small Tafel slope of 40 mV/dec observed here is desirable to drive a large catalytic current density at low overpotential. Noticeably, the linear region of the Tafel plot of the $CoSe_2$ nanoparticle/CP electrode extends to a high current density of ~80 mA/cm^2, so the catalyst offers exceptional performance, especially at higher overpotentials. In experiment, the logarithmic current density usually deviates from linear dependence at high overpotentials,[18−20] which is strongly influenced by evolved hydrogen bubbles limiting the available surface area or mass transport.[8,20] We observed the the $CoSe_2$ nanoparticle coating significantly improves the release of produced hydrogen gas from CP (see Movies S1 and S2), which is a highly desired property for the practical application of HER catalysts. The exchange current density of $CoSe_2$ nanoparticle/CP electrodes is ~$(4.9 \pm 1.4) \times 10^{-6}$ A/cm^2, which is about 2 orders of magnitude larger than the value of $(5.9 \pm 1.7) \times 10^{-8}$ A/cm^2 for $CoSe_2$ films. Typically, the exchange current density is expected to be proportional to catalytically active surface area. An alternative approach to estimate the effective surface area is to measure the capacitance of the double layer at the solid–liquid interface with cyclic voltammetry,[46] as shown in Figure 3c,d. The capacitance of $CoSe_2$ nanoparticle/CP electrode is 14.1 mF/cm^2. In contrast, the capacitance of smooth $CoSe_2$ film is 22 μF/cm^2, within the typical range for a flat electrode.[47] Accordingly, the roughness factor of $CoSe_2$ nanoparticle/CP electrode is ~640. The electrochemical surface area serves as an approximate guide for surface roughness within an order-of-magnitude accuracy.[48] Therefore, the large exchange current density of the $CoSe_2$ nanoparticle/CP electrode is associated with its high surface area.

Stability is a critical aspect in the development of electrocatalysts. To probe the durability of the catalyst in acidic environment, long-term potential cycling was performed by taking continuous cyclic voltammograms at an accelerated scanning rate of 100 mV/s for 5000 cycles. We set the lower potential limit to drive a large cathodic current density of 200 mA/cm^2. As shown in Figure 4a, the polarization curve of a

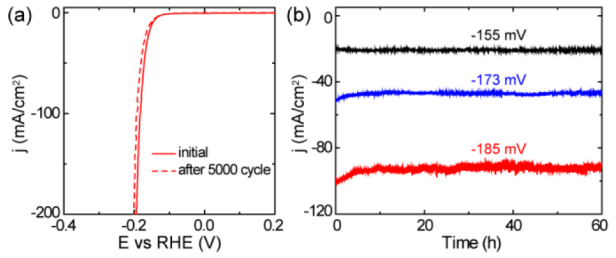

Figure 4. (a) Stability tests of $CoSe_2$ NP/CP catalyst through potential cycling, in which the polarization curves before and after 5000 potential cycles are displayed. (b) Time dependence of cathodic current density during electrolysis over 60 h at fixed overpotentials of −155, −173, and −185 mV (after *iR* correction), respectively.

$CoSe_2$ nanoparticle/CP catalyst after 5000 cycles overlays almost exactly with the initial one, with negligible loss of cathodic current. This confirms the catalyst is highly stable to withstand accelerated degradation. Furthermore, the practical operation of the catalyst is examined by electrolysis at fixed potentials over extended periods. At a lower overpotential of 155 mV, the catalyst current density remains stable at ~20 mA/cm^2 for electrolysis over 60 h. At higher overpotentials to drive high current densities of ~50 and ~100 mA/cm^2, a little loss in cathodic current density of less than 10% is observed in the $CoSe_2$ nanoparticle/CP electrodes during the first several hours. The catalytic current then fully stabilized for the rest of the potentiostatic electrolysis. This exceptional durability shows promise for practical applications of the catalysts over the long term.

In conclusion, we have developed a facile and flexible synthesis approach to grow a $CoSe_2$ nanoparticulate film over 3D electrodes. The $CoSe_2$ catalyst grown on carbon fiber paper exhibits excellent HER activity, with a small Tafel slope of ~40 mV/dec. The catalyst is able to drive large cathodic current at low overpotential and stably function over an extended period. This material synthesis approach allows facile preparation of advanced $CoSe_2$ HER catalysts on various electrodes, which may be readily integrated with many solar water-splitting devices.

■ ASSOCIATED CONTENT

Ⓢ Supporting Information

Complete experimental details, additional characterizations, analyses of HER data, and movies of the catalyst in operation. This material is available free of charge via the Internet at http://pubs.acs.org.

■ AUTHOR INFORMATION

Corresponding Author

yicui@stanford.edu

Notes

The authors declare no competing financial interest.

■ ACKNOWLEDGMENTS

We acknowledge the support by the U.S. Department of Energy, Office of Basic Energy Sciences, Materials Sciences and Engineering Division, under Contract DE-AC02-76-SFO0515.

■ REFERENCES

(1) Gray, H. B. *Nat. Chem.* **2009**, *1*, 7.
(2) Lewis, N. S.; Nocera, D. G. *Proc. Natl. Acad. Sci. U.S.A.* **2006**, *103*, 15729−15735.
(3) Zheng, Y.; Jiao, Y.; Ge, L.; Jaroniec, M.; Qiao, S. Z. *Angew. Chem., Int. Ed.* **2013**, *52*, 3110−3116.
(4) Hinnemann, B.; Moses, P. G.; Bonde, J.; Jørgensen, K. P.; Nielsen, J. H.; Horch, S.; Chorkendorff, I.; Nørskov, J. K. *J. Am. Chem. Soc.* **2005**, *127*, 5308−5309.
(5) Jaramillo, T. F.; Jørgensen, K. P.; Bonde, J.; Nielsen, J. H.; Horch, S.; Chorkendorff, I. *Science* **2007**, *317*, 100−102.
(6) Li, Y.; Wang, H.; Xie, L.; Liang, Y.; Hong, G.; Dai, H. *J. Am. Chem. Soc.* **2011**, *133*, 7296−7299.
(7) Chen, Z.; Cummins, D.; Reinecke, B. N.; Clark, E.; Sunkara, M. K.; Jaramillo, T. F. *Nano Lett.* **2011**, *11*, 4168−4175.
(8) Merki, D.; Vrubel, H.; Rovelli, L.; Fierro, S.; Hu, X. *Chem. Sci.* **2012**, *3*, 2515−2525.
(9) Kibsgaard, J.; Chen, Z.; Reinecke, B. N.; Jaramillo, T. F. *Nat. Mater.* **2012**, *11*, 963−969.
(10) Lukowski, M. A.; Daniel, A. S.; Meng, F.; Forticaux, A.; Li, L.; Jin, S. *J. Am. Chem. Soc.* **2013**, *135*, 10274−10277.
(11) Merki, D.; Fierro, S.; Vrubel, H.; Hu, X. *Chem. Sci.* **2011**, *2*, 1262−1267.
(12) Chang, Y.-H.; Lin, C.-T.; Chen, T.-Y.; Hsu, C.-L.; Lee, Y.-H.; Zhang, W.; Wei, K.-H.; Li, L.-J. *Adv. Mater.* **2013**, *25*, 756−760.
(13) Kong, D.; Wang, H.; Cha, J. J.; Pasta, M.; Koski, K. J.; Yao, J.; Cui, Y. *Nano Lett.* **2013**, *13*, 1341−1347.
(14) Wang, H.; Kong, D.; Johanes, P.; Cha, J. J.; Zheng, G.; Yan, K.; Liu, N.; Cui, Y. *Nano Lett.* **2013**, *13*, 3426−3433.
(15) Voiry, D.; Yamaguchi, H.; Li, J.; Silva, R.; Alves, D. C. B.; Fujita, T.; Chen, M.; Asefa, T.; Shenoy, V. B.; Eda, G.; Chhowalla, M. *Nat. Mater.* **2013**, *12*, 850−855.
(16) Vrubel, H.; Hu, X. *Angew. Chem., Int. Ed.* **2012**, *124*, 12875−12878.
(17) Chen, W. F.; Wang, C. H.; Sasaki, K.; Marinkovic, N.; Xu, W.; Muckerman, J. T.; Zhu, Y.; Adzic, R. R. *Energy Environ. Sci.* **2013**, *6*, 943−951.
(18) Chen, W.-F.; Sasaki, K.; Ma, C.; Frenkel, A. I.; Marinkovic, N.; Muckerman, J. T.; Zhu, Y.; Adzic, R. R. *Angew. Chem., Int. Ed.* **2012**, *51*, 6131−6135.
(19) Popczun, E. J.; McKone, J. R.; Read, C. G.; Biacchi, A. J.; Wiltrout, A. M.; Lewis, N. S.; Schaak, R. E. *J. Am. Chem. Soc.* **2013**, *135*, 9267−9270.
(20) Cao, B.; Veith, G. M.; Neuefeind, J. C.; Adzic, R. R.; Khalifah, P. G. *J. Am. Chem. Soc.* **2013**, *135*, 19186−19192.
(21) Kong, D.; Cha, J. J.; Wang, H.; Lee, H. R.; Cui, Y. *Energy Environ. Sci.* **2013**, *6*, 3553−3558.
(22) Zhu, L.; Teo, M.; Wong, P. C.; Wong, K. C.; Narita, I.; Ernst, F.; Mitchell, K. A. R.; Campbell, S. A. *Appl. Catal. A: General* **2010**, *386*, 157−165.
(23) Feng, Y.; He, T.; Alonso-Vante, N. *Electrochim. Acta* **2009**, *54*, 5252−5256.
(24) Feng, Y. J.; He, T.; Alonso-Vante, N. *Fuel Cells* **2010**, *10*, 77−83.
(25) Xu, Y.-F.; Gao, M.-R.; Zheng, Y.-R.; Jiang, J.; Yu, S.-H. *Angew. Chem., Int. Ed.* **2013**, *52*, 8546−8550.
(26) Sun, Y.; Liu, C.; Grauer, D. C.; Yano, J.; Long, J. R.; Yang, P.; Chang, C. J. *J. Am. Chem. Soc.* **2013**, *135*, 17699−17702.
(27) Cabán-Acevedo, M.; Faber, M. S.; Tan, Y.; Hamers, R. J.; Jin, S. *Nano Lett.* **2012**, *12*, 1977−1982.
(28) Boettcher, S. W.; Warren, E. L.; Putnam, M. C.; Santori, E. A.; Turner-Evans, D.; Kelzenberg, M. D.; Walter, M. G.; McKone, J. R.; Brunschwig, B. S.; Atwater, H. A.; Lewis, N. S. *J. Am. Chem. Soc.* **2011**, *133*, 1216−1219.
(29) McKone, J. R.; Warren, E. L.; Bierman, M. J.; Boettcher, S. W.; Brunschwig, B. S.; Lewis, N. S.; Gray, H. B. *Energy Environ. Sci.* **2011**, *4*, 3573−3583.
(30) Hou, Y.; Abrams, B. L.; Vesborg, P. C. K.; Björketun, M. E.; Herbst, K.; Bech, L.; Setti, A. M.; Damsgaard, C. D.; Pedersen, T.; Hansen, O.; Rossmeisl, J.; Dahl, S. r.; Nørskov, J. K.; Chorkendorff, I. *Nat. Mater.* **2011**, *10*, 434−438.
(31) Liu, C.; Tang, J.; Chen, H. M.; Liu, B.; Yang, P. *Nano Lett.* **2013**, *13*, 2989−2992.
(32) Dai, P.; Xie, J.; Mayer, M. T.; Yang, X.; Zhan, J.; Wang, D. *Angew. Chem., Int. Ed.* **2013**, *52*, 11119−11123.
(33) Chen, S.; Duan, J.; Jaroniec, M.; Qiao, S. Z. *Angew. Chem., Int. Ed.* **2013**, *52*, 13567−13570.
(34) Sun, R.; Chan, M. K. Y.; Ceder, G. *Phys. Rev. B* **2011**, *83*, 235311.
(35) Chao, Y.-S.; Tsai, D.-S.; Wu, A.-P.; Tseng, L.-W.; Huang, Y.-S. *Int. J. Hydrogen Energy* **2013**, *38*, 5655−5664.
(36) Anastassakis, E. *Solid State Commun.* **1973**, *13*, 1297−1301.
(37) Carroll, P. J.; Lannin, J. S. *Solid State Commun.* **1981**, *40*, 81−84.
(38) Yang, J.; Cheng, G.-H.; Zeng, J.-H.; Yu, S.-H.; Liu, X.-M.; Qian, Y.-T. *Chem. Mater.* **2001**, *13*, 848−853.
(39) Ogawa, S. *J. Appl. Phys.* **1979**, *50*, 2308−2311.
(40) Tossell, J. A.; Vaughan, D. J.; Burdett, J. K. *Phys. Chem. Miner.* **1981**, *7*, 177−184.
(41) Bither, T. A.; Bouchard, R. J.; Cloud, W. H.; Donohue, P. C.; Siemons, W. J. *Inorg. Chem.* **1968**, *7*, 2208−2220.
(42) van der Heide, H.; Hemmel, R.; van Bruggen, C. F.; Haas, C. *J. Solid State Chem.* **1980**, *33*, 17−25.
(43) Adachi, K.; Matsui, M.; Omata, Y. *J. Phys. Soc. Jpn.* **1981**, *50*, 83.
(44) Conway, B. E.; Tilak, B. V. *Electrochim. Acta* **2002**, *47*, 3571−3594.
(45) Pentland, N.; Bockris, J. O. M.; Sheldon, E. *J. Electrochem. Soc.* **1957**, *104*, 182−194.
(46) Trasatti, S.; Petrii, O. A. *J. Electroanal. Chem.* **1992**, *327*, 353−376.
(47) Conway, B. E.; Birss, V.; Wojtowicz, J. *J. Power Sources* **1997**, *66*, 1−14.
(48) McCrory, C. C. L.; Jung, S.; Peters, J. C.; Jaramillo, T. F. *J. Am. Chem. Soc.* **2013**, *135*, 16977−16987.